Structural, Spectroscopic, and Electrochemical Studies of Binuclear Manganese(II) Complexes of Bis(pentadentate) Ligands Derived from Bis(1,4,7-triazacyclononane) Macrocycles

Suzanne J. Brudenell,[†] Leone Spiccia,*[,†] Alan M. Bond,[†] Gary D. Fallon,[†] David C. R. Hockless,[‡] George Lazarev,[§] Peter J. Mahon,[†] and Edward R. T. Tiekink[||]

Department of Chemistry, Monash University, Clayton, Victoria 3168, Australia, Research School of Chemistry, Australian National University, Canberra, ACT 2601, Australia, Department of Physics, Monash University, Clayton, Victoria 3168, Australia, and Department of Chemistry, The University of Adelaide, Adelaide, South Australia 5005, Australia

Received December 18, 1998

Structural, electrochemical, ESR, and H_2O_2 reactivity studies are reported for $[Mn(dmptacn)Cl]ClO_4$ (**1**, dmptacn = 1,4-bis(2-pyridylmethyl)-1,4,7-triazacyclononane) and binuclear complexes of bis(pentadentate) ligands, generated by attaching 2-pyridylmethyl arms to each secondary nitrogen in bis(1,4,7-triazacyclononane) macrocycles and linked by ethyl (tmpdtne, $[Mn_2(tmpdtne)Cl_2](ClO_4)_2 \cdot 2DMF$, **2**), propyl (tmpdtnp, $[Mn_2(tmpdtnp)Cl_2](ClO_4)_2 \cdot 3H_2O$, **3**), butyl (tmpdtnb, $[Mn_2(tmpdtnb)Cl_2](ClO_4)_2 \cdot DMF \cdot 2H_2O$, **4**), *m*-xylyl (tmpdtn-*m*-X, $[Mn_2(tmpdtn\text{-}m\text{-}X)Cl_2](ClO_4)_2$, **5**) and 2-propanol (tmpdtnp-OH, $[Mn_2(tmpdtnp\text{-}OH)Cl_2](ClO_4)_2$, **6**) groups. **1** crystallizes in the orthorhombic space group $P2_12_12_1$ (No. 19) with $a = 7.959(7)$ Å, $b = 12.30(1)$ Å, and $c = 21.72(2)$ Å; **2**, in the monoclinic space group $P2_1/c$ (No. 14) with $a = 11.455(4)$ Å, $b = 15.037(6)$ Å, $c = 15.887(4)$ Å, and $\beta = 96.48(2)°$; **3**, in the monoclinic space group $P2_1/c$ (No. 14) with $a = 13.334(2)$ Å, $b = 19.926(2)$ Å, $c = 18.799(1)$ Å, and $\beta = 104.328(8)°$; and $[Mn_2(tmpdtnb)Cl_2](ClO_4)_2 \cdot 4DMF \cdot 3H_2O$ (**4′**), in the monoclinic space group $P2_1/n$ (No. 14) with $a = 13.361(3)$ Å, $b = 16.807(5)$ Å, $c = 14.339(4)$ Å, and $\beta = 111.14(2)°$. Significant distortion of the Mn(II) geometry is evident from the angle subtended by the five-membered chelate (ca. 75°) and the angles spanned by trans donor atoms (<160°). The Mn geometry is intermediate between octahedral and trigonal prismatic, and for complexes **2**−**4**, there is a systematic increase in M···M distance with the length of the alkyl chain. Cyclic and square-wave voltammetric studies indicate that **1** undergoes a $1e^-$ oxidation from Mn(II) to Mn(III) followed by a further oxidation to Mn^{IV} at a significantly more positive potential. The binuclear Mn(II) complexes **2**−**5** are oxidized to the Mn(III) state in two unresolved $1e^-$ processes $\{Mn^{II}{}_2 \rightarrow Mn^{II}Mn^{III} \rightarrow Mn^{III}{}_2\}$ and then to the Mn^{IV} state $\{Mn^{III}{}_2 \rightarrow Mn^{III}Mn^{IV} \rightarrow Mn^{IV}{}_2\}$. For **2**, the second oxidation process was partially resolved into two $1e^-$ oxidation processes under the conditions of square-wave voltammetry. In the case of **6**, initial oxidation to the $Mn^{III}{}_2$ state occurs in two overlapping $1e^-$ processes as was found for **2**−**5**, but this complex then undergoes two further clearly separated $1e^-$ oxidation processes to the $Mn^{III}Mn^{IV}$ state at +0.89 V and the $Mn^{IV}{}_2$ state at +1.33 V (vs Fc/Fc^+). This behavior is attributed to formation of an alkoxo-bridged complex. Complexes **1**−**6** were found to catalyze the disproportionation of H_2O_2. Addition of H_2O_2 to **2** generated an oxo-bridged mixed-valent $Mn^{III}Mn^{IV}$ intermediate with a characteristic 16-line ESR signal.

Introduction

Interest in manganese complexes of varying nuclearities continues to be stimulated by the presence of manganese at the active sites of biological systems such as photosystem II in green plants, ribonucleotide reductase, superoxide dismutase, and the Mn catalases (see refs 1−10 and references therein), the variability in magnetic behavior of polynuclear manganese clusters, which for some systems has been exploited in the development of information storage devices,[11] and the use of such complexes as catalysts for bleaching and organic synthesis.[12]

The manganese coordination chemistry of the tridentate macrocycle 1,4,7-triazacyclononane (tacn), its 1,4,7-trimethyl

* Corresponding author. E-mail: leone.spiccia@sci.monash.edu.au.
[†] Department of Chemistry, Monash University.
[‡] Australian National University.
[§] Department of Physics, Monash University.
[||] The University of Adelaide.

(1) Wieghardt, K. *Angew. Chem., Int. Ed. Engl.* **1989**, *28*, 1153.
(2) Pecoraro, V. L. In *Manganese Redox Enzymes*; Larson, E. J., Pecoraro, V. L., Eds.; VCH: New York, 1992; Chapter 1, p 1.
(3) Thorp, H. H., Pecoraro, V. L., Eds. *Mechanistic Bioinorganic Chemistry*; Advances in Chemistry Series 246; American Chemical Society: Washington, DC, 1995.
(4) Yachandra, V. K.; Sauer, K.; Klein, M. P. *Chem. Rev.* **1996**, *96*, 2927.
(5) Rüttinger, W.; Dismukes, G. C. *Chem. Rev.* **1997**, *97*, 1.
(6) Tommos, C.; Babcock, G. T. *Acc. Chem. Res.* **1998**, *31*, 18.
(7) Pecoraro, V. L.; Baldwin, M. J.; Gelasco, A. *Chem. Rev.* **1994**, *94*, 807.
(8) Dismukes, G. C. *Chem. Rev.* **1996**, *96*, 2929.
(9) Ludwig, M. L.; Metzger, A. L.; Pattridge, K. A.; Stallings, W. C. *J. Biol. Chem.* **1991**, *219*, 335.
(10) Riley, D. P.; Lennon, P. J.; Neumann, W. L.; Weiss, R. H. *J. Am. Chem. Soc.* **1997**, *119*, 6522.
(11) (a) Sessoli, R.; Tsai, H.-L.; Schake, A. R.; Wang, S.; Vincent, J. B.; Folding, K.; Gatteschi, D.; Christou, G.; Hendrickson, D. N. *J. Am. Chem. Soc.* **1993**, *115*, 1804. (b) Chudnovsky, E. M. *Science* **1996**, *274*, 938. (c) Aubin, S. M. J.; Sun, Z.; Guzei, I. A.; Rheingold, A. L.; Christou, G.; Hendrickson, D. N. *Chem. Commun.* **1997**, 2239.

10.1021/ic9814470 CCC: $19.00
Published on Web 02/11/2000

analogue (Me_3tacn), derivatives bearing pendant coordinating groups, and some bis(tridentate) macrocycles incorporating tacn has attracted significant attention,[13−29] since the first reports of polynuclear Mn complexes incorporating such ligands in the mid-1980s. Some of the products have been described as models for the polynuclear manganese cluster in the "oxygen-evolving complex" of photosystem II, and others, as models for binuclear Mn biosites. An attractive feature of tacn-based ligands is their ability to form thermodynamically stable but redox-active Mn(II) compounds,[18] which can be converted into higher-valent complexes. Polynuclear oxo, oxo−carboxylato, oxo−peroxo, phenoxo−carboxylato, hydroxo−carboxylato, and oxo−boronato bridged complexes with varying Mn oxidation states are among those reported, and mixed-valent polynuclear complexes are not uncommon.[13−16,18−29] Complexes with an (oxo/hydroxo)bis(carboxylato)dimanganese core have been of interest because such a core is found at the active site of some catalases and ribonucleotide reductase. The peroxo-bridged complex $[(Me_3tacn)_2Mn_2(\mu_2\text{-}O)_2(\mu\text{-}O_2)]^{2+}$ also has particular relevance to the function of these metalloenzymes.[21]

Manganese complexes derived from Me_3tacn and the bis(1,4,7-triazacyclononane) ligand 1,2-bis(4, 7-dimethyl-1,4,7-triazacyclonon-1-yl)ethane (Me_4dtne) were recently shown to enhance the low-temperature bleaching of stains by hydrogen peroxide.[12a] The mixed-valent complex $[Mn^{III}Mn^{IV}(\mu\text{-}O)_2(\mu\text{-}CH_3COO)Me_4dtne]^{2+}$ was found to be particularly effective. It exhibits a 16-line ESR spectrum typical of μ-oxo mixed-valent $Mn^{III}Mn^{IV}$ complexes.

Scheme 1

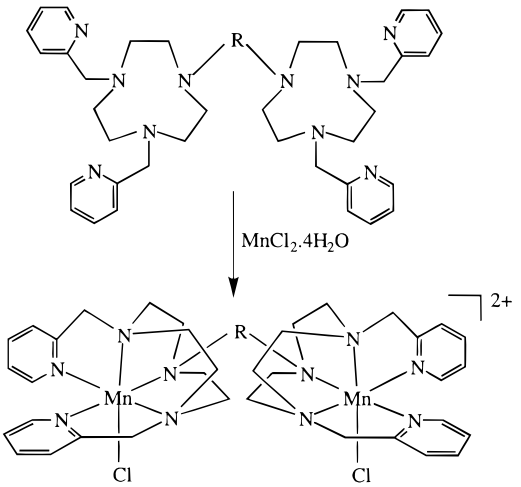

(**2**) R = CH_2CH_2
(**3**) R = $CH_2CH_2CH_2$
(**4**) R = $CH_2CH_2CH_2CH_2$
(**5**) R = *m*-xylyl
(**6**) R = $CH_2CH(OH)CH_2$

Although many dimanganese complexes have been studied to increase the understanding of the role and mechanism of action of manganese in dioxygen chemistry, binuclear manganese complexes incorporating bis(1,4,7-triazacyclononane) ligands are relatively unexplored. In this paper, we report structural, physicochemical, and electrochemical properties of a series of binuclear Mn(II) complexes based on the bis(pentadentate) ligands that are formed by attaching 2-pyridylmethyl pendant groups to each secondary nitrogen in bis(1,4,7-triazacyclononane) macrocycles (see Scheme 1). Since many of the previously reported Mn compounds that enhance hydrogen peroxide disproportionation incorporate tridentate blocking ligands and multiple bridges between Mn centers, we were surprised to find that our "unsupported" complexes were also active. Preliminary solution studies of the reactions of these complexes with hydrogen peroxide reveal interesting variations in reactivity with the spacer separating the two ligand compartments, which are observable by UV-visible and ESR spectroscopy.

Experimental Section

Materials. Reagent or AR grade chemicals were used in this study. Published methods were used to prepare 1,4-bis(2-pyridylmethyl)-1,4,7-triazacyclononane (dmptacn),[30] 1,2-bis[4,7-bis(2-pyridylmethyl)-1,4,7-triazacyclonon-1-yl]ethane (tmpdtne),[31] 1,3-bis[4,7-bis(2-pyridylmethyl)-1,4,7-triazacyclonon-1-yl]propane (tmpdtnp),[31] 1,4-bis[4,7-bis(2-pyridylmethyl)-1,4,7-triazacyclonon-1-yl]butane (tmpdtnb),[31] 1,3-bis[4,7-bis(2-pyridylmethyl)-1,4,7-triazacyclonon-1-ylmethyl]benzene (tmpdtn-*m*-X)[32] and 1,3-bis[4,7-bis(2-pyridylmethyl)-1,4,7-triazacyclonon-1-yl]-2-propanol (tmpdtnp-OH).[32]

Caution! *Although no problems were encountered in this work, transition metal perchlorates are potentially explosive. They should be prepared in small quantities and handled with care.*

Physical Measurements. Infrared spectra were measured on a Perkin-Elmer 1600 FTIR spectrometer as KBr pellets. Electron microprobe analyses were made with a JEOL JSM-1 scanning electron

(12) (a) Hage, R.; Iburg, J. E.; Kerschner, J.; Koek, J. H.; Lempers, E. L. M.; Martens, R. J.; Racherla, U. S.; Russell, S. W.; Swarthoff, T.; van Vliet, M. R. P.; Warnaar, J. B.; van der Wolf, L.; Krljen, B. *Science* **1994**, *369*, 637. (b) de Vos, D. E.; Ben, T. *J. Organomet. Chem.* **1996**, *520*, 195. (c) Zondervan, C.; Hage, R.; Ferigna, B. L. *Chem. Commun.* **1997**, 419.
(13) Wieghardt, K.; Bossek, U.; Ventur, D.; Weiss, J. *Chem. Commun.* **1985**, 347.
(14) Wieghardt, K.; Bossek, U.; Bonvoisin, J.; Beauvillain, P.; Girerd, J. J.; Nuber, B.; Weiss, J.; Heinze, J. *Angew. Chem., Int. Ed. Engl.* **1986**, *25*, 1030.
(15) Wieghardt, K.; Tolksdorf, I.; Herrmann, W. *Inorg. Chem.* **1985**, *24*, 1230.
(16) Wieghardt, K.; Bossek, U.; Zsolnai, L.; Huttner, G.; Blondin, G.; Girerd J.-J.; Babonneau, F. *Chem. Commun*. **1987**, 651.
(17) Wieghardt, K.; Schoffman, E.; Nuber, B.; Weiss, J. *Inorg. Chem.* **1986**, *25*, 4877.
(18) Chaudhuri, P.; Wieghardt, K. *Prog. Inorg. Chem.* **1987**, *35*, 329.
(19) Wieghardt, K.; Bossek, U.; Nuber, B.; Weiss, J.; Bonvoisin, J.; Corbella, M.; Vitols, S. E.; Girerd, J. J. *J. Am. Chem. Soc.* **1988**, *110*, 7398.
(20) Chang, H.-R.; Diril, H.; Nilges, M. J.; Zhang, X.; Potenza, J. A.; Schugar, H. J.; Hendrickson, D. N.; Isied, S. S. *J. Am. Chem. Soc.* **1988**, *110*, 62
(21) Bossek, U.; Weyhermuller, T.; Wieghardt, K.; Nuber, B.; Weiss, J. *J. Am. Chem. Soc.* **1990**, *112*, 6387.
(22) Diril, H.; Chang, H.-R.; Nilges, M. J.; Zhang, X.; Potenza, J. A.; Schugar, H. J.; Isied, S. S.; Hendrickson, D. N. *J. Am. Chem. Soc.* **1989**, *111*, 5102.
(23) Bossek, U.; Weyermüller, T.; Wieghardt, K.; Huber, B.; Weiss, J. *J. Am. Chem. Soc*. **1990**, *112*, 6387.
(24) Bossek U.; Saher, M.; Weyermüller, T.; Wieghardt, K. *Chem. Commun*. **1992**, 1780.
(25) Koek, J. H.; Russell, S. W.; van der Wolf, L.; Hage, R.; Warnaar, J. B.; Spek, A. L.; Kerschner, J.; Delpizzo, L. *J. Chem. Soc., Dalton Trans.* **1996**, 353.
(26) Darovsky, A.; Kererashvili, V.; Coppens, P.; Weyermüller, T.; Hummel, H.; Wieghardt, K. *Inorg. Chem.* **1996**, *35*, 6916.
(27) Bossek, U.; Hummel, H.; Weyermüller, T.; Wieghardt, K.; Russell, S.; van der Wolf, L.; Kolb, U. *Angew. Chem., Int. Ed. Engl.* **1996**, *35*, 1552.
(28) Fallon, G. D.; McLachlan, G. A.; Moubaraki, B.; Murray, K. S.; O'Brien, L.; Spiccia, L. *J. Chem. Soc., Dalton Trans*. **1997**, 2765.
(29) Hummel, H.; Bill, E.; Weyhermuller, T.; Wieghardt, K.; Davydov, R.; Russell, S. *Poster presented at the Eighth International Conference on Bioinorganic Chemistry*, Yokohama, Japan, 1997.
(30) McLachlan, G. A.; Fallon, G. D.; Martin, R. L.; Moubaraki, B.; Murray, K. S.; Spiccia, L. *Inorg. Chem.* **1994**, *33*, 4663.
(31) Brudenell, S. J.; Spiccia, L.; Tiekink, E. R. T. *Inorg. Chem*. **1996**, *35*, 1974.
(32) Brudenell, S. J.; Spiccia, L.; Bond, A. M.; Hockless, D. C. R.; Tiekink, E. R. T. *Inorg. Chem.* **1998**, *37*, 3705.

microscope through an NEC X-ray detector and pulse processing system connected to a Packard multichannel analyzer. Microanalyses were carried out by the Chemical and Micro-Analytical Services (CMAS), Melbourne, Australia. Room-temperature magnetic moments were determined by the Faraday method. Diamagnetic corrections were made using Pascal's constants. Low-temperature magnetic susceptibility measurements were carried out on a Quantum Design MPMS SQUID magnetometer as described previously.[12] Electrospray ionization mass spectra were recorded either on a Micromass Platform QMS with an electrospray source or on a Bruker BioApex 47e FTMS with a 4−7 T superconducting magnet and an Analytica electrospray source.

ESR spectra were measured on a Bruker ECS 106 spectrometer as frozen (99 K) DMF solutions using a concentration of 0.5 mM. To follow the reactivity of Mn(II) complexes toward hydrogen peroxide, solutions of the complexes were allowed to react with H_2O_2 in the ESR tubes for a particular length of time. The solutions were frozen in liquid nitrogen to quench the reaction and enable the ESR spectra to be recorded. Following measurement of the ESR spectra, the solutions were left to warm to room temperature and allowed to react further. The solutions were frozen again and the ESR spectra re-recorded.

Electronic spectra were recorded on a Cary 3 spectrophotometer. Changes in UV−visible spectra that occurred following addition of aqueous hydrogen peroxide to the Mn(II) complexes (∼5 mM in DMF) were monitored as a function of time using the kinetics accessory and software package of the spectrophotometer.

Cyclic, square-wave, and steady-state voltammograms were recorded on a Cypress CS 1090 system in dry, nitrogen-deoxygenated acetonitrile solutions (∼0.5 mM) with tetrabutylammonium perchlorate (0.1 M) as the supporting electrolyte. A platinum auxiliary electrode and an Ag/Ag^+ (10 mM $AgNO_3$) reference electrode were used in combination with either a platinum macrodisk working electrode ($r = 0.8$ mm) for cyclic and square-wave voltammetry or a platinum microelectrode ($r = 25\ \mu$m) for near-steady-state voltammetry conducted in an aluminum Faraday cage. Potentials are reported relative to the ferrocene/ferrocenium (Fc/Fc^+) couple. Reversible redox potentials ($E_{1/2}$ values) were determined from the cyclic voltammograms of the chemically reversible processes as the midpoint between the oxidation (E_p^{ox}) and reduction (E_p^{red}) peak potentials, $E_{1/2} = {}^1/_2(E_p^{ox} + E_p^{red})$. Confirmation of electrochemical reversibility was established by verifying that the $E_{1/2}$ values calculated from a CV experiment were equal to the peak potentials, E_p, of square-wave voltammograms. The $E_{1/2}$ values were also equal to the $E_{1/2}$ values measured under steady-state conditions at a microelectrode as the potential at half the limiting current value ($I_L/2$). The diffusion coefficient (D) was calculated from the limiting current (I_L) and the use of the relationship $I_L = 4nFCDr$, where F = Faraday's constant, C = concentration, r = radius of the microdisk electrode, and n = the number of electrons in the charge-transfer step.

Synthesis of complexes. (a) [Mn(dmptacn)Cl]ClO_4 (1). Dmptacn (1.50 g, 4.8 mmol) was dissolved in MeOH (20 mL), and $MnCl_2·4H_2O$ (0.95 g, 4.8 mmol) was added. A white solid precipitated on addition of $NaClO_4$ (1.0 g) to this solution. Recrystallization from an H_2O/DMF mixture afforded rectangular, colorless crystals suitable for X-ray crystallography (yield 1.05 g, 44%). Anal. Calc for $[Mn(C_{18}H_{25}N_5)Cl]ClO_4$: C, 48.4; H, 5.6; N, 15.7. Found: C, 48.5; H, 5.7; N, 15.7. Electron microprobe: Cl:Mn ratio 2:1. Selected IR bands (KBr, cm^{-1}): 3336m, 2917m, 2858m, 1606m, 1491m, 1441m, 1144m, 1088vs, 1017m, 761m, 626s. Magnetic moment: μ_{eff}(296 K) = 5.92 μ_B.

(b) $[Mn_2(tmpdtne)Cl_2](ClO_4)_2·2DMF$ (2). Tmpdtne (1.50 g, 2.3 mmol) was dissolved in MeOH (20 mL), and a slight excess of $MnCl_2·4H_2O$ (0.96 g, 4.9 mmol) was added. The addition of $NaClO_4$ (1.0 g) to this brown solution resulted in the precipitation of a light brown solid. This solid was recrystallized from an H_2O/DMF mixture to afford small, rectangular, colorless crystals suitable for X-ray crystallography (yield 1.11 g, 41%). Anal. Calc. for $[Mn_2(C_{38}H_{52}N_{10})Cl_2](ClO_4)_2·2DMF$: C, 45.0; H, 5.6; N, 14.3. Found: C, 45.0; H, 5.6; N, 14.3. Electron microprobe: Cl:Mn ratio 2:1. Selected IR bands (KBr, cm^{-1}): 2917m, 2858m, 1665m, 1606m, 1491m, 1441m, 1367m, 1299m, 1144m, 1088vs, 1017m, 761m, 626s. Magnetic moment: μ_{eff}(296 K) = 5.92 μ_B per Mn(II).

(c) $[Mn_2(tmpdtnp)Cl_2](ClO_4)_2·3H_2O$ (3). The method used to prepare **2** was followed except that 1.5 g (2.27 mmol) of tmpdtnp and 0.94 g (4.77 mmol) of $MnCl_2·4H_2O$ were used. Recrystallization from a DMF/H_2O mixture gave the product as a trihydrate (yield 1.21 g, 45%). Colorless crystals suitable for X-ray crystallography were obtained on slow evaporation of a DMF/H_2O solution of the compound. Anal. Calc for $[Mn_2(C_{39}H_{54}N_{10})Cl_2](ClO_4)_2·3H_2O$: C, 42.7; H, 5.5; N, 12.8. Found: C, 43.3; H, 5.7; N, 13.2. Electron microprobe: Cl:Mn ratio 2:1. Selected IR bands (KBr, cm^{-1}): 3412vs, 2890w, 2853w, 1638m, 1607s, 1494m, 1442m, 1384m, 1299m, 1116s, 1083vs, 1013s, 780s, 628s. Magnetic moment: μ_{eff}(296 K) = 5.94 μ_B per Mn(II).

(d) $[Mn_2(tmpdtnb)Cl_2](ClO_4)_2·DMF.2H_2O$ (4). The synthesis was as for **2** except that 1.3 g (1.93 mmol) of tmpdtnb and 0.80 g (4.06 mmol) of $MnCl_2·4H_2O$ were used. Recrystallization from a DMF/H_2O mixture gave the product as a mono(dimethylformamide) diaqua solvate for which the analytical data given below were collected (yield 1.16 g, 50%). Colorless crystals of the tetrakis(dimethylformamide) triaqua solvate, **4′**, suitable for X-ray crystallography were obtained on slow evaporation of a DMF/H_2O solution of the compound. Anal. Calc for $[Mn_2(C_{40}H_{56}N_{10})Cl_2](ClO_4)_2.DMF·2H_2O$: C 44.3, H 5.8, N 13.2; found: C 44.2, H 5.7, N 13.3. Electron microprobe: Cl:Mn ratio 2:1. Selected IR bands (KBr, cm^{-1}): 3452s, 2925m, 2856m, 1668vs, 1606s, 1495m, 1441m, 1390m, 1309m, 1150m, 1102vs, 1015s, 766s, 624s. Magnetic moment: μ_{eff}(296 K) = 5.81 μ_B per Mn(II).

(e) $[Mn_2(tmpd$tn-m-X$)Cl_2](ClO_4)_2.6H_2O$ (5). The synthesis was as for **2** except that 0.90 g (1.24 mmol) of tmpdtn-*m*-X and 0.52 g (2.61 mmol) of $MnCl_2·4H_2O$ were used. The product appeared as a brown solid after recrystallization of the initial brown precipitate from a mixture of DMF/H_2O (yield 0.59 g, 38%). Anal. Calc. for $[Mn_2(C_{44}H_{56}N_{10})Cl_2](ClO_4)_2·6H_2O$: C, 43.6; H, 5.6; N, 11.6. Found: C, 43.5; H, 5.0; N, 11.6. Electron microprobe: Cl:Mn ratio 2:1. ESI mass spectrum (CH_3CN), *m/z*: 1005.2, $\{[Mn_2LCl_2]ClO_4\}^+$; 452.2, $\{Mn_2LCl_2\}^{2+}$. Selected IR bands (KBr, cm^{-1}): 3417s, 3066w, 2919w, 2857m, 1657m, 1608s, 1486w, 1442m, 1384m, 1296m, 1090vs, 1016s, 763s, 626s. Magnetic moment: μ_{eff}(293 K) = 5.83 μ_B per Mn(II).

(f) $[Mn_2(tmpdtnp-OH)Cl_2](ClO_4)_2·2H_2O$ (6). The method used to prepare **2** was followed except that 1.5 g (2.3 mmol) of tmpdtnp-OH and 0.94 g (4.8 mmol) of $MnCl_2·4H_2O$ were used. Colorless crystals of **6** were obtained on recrystallization from a CH_3CN/H_2O mixture (yield 1.12 g, 45%). Anal. Calc for $[Mn_2(C_{39}H_{54}N_{10}O)Cl_2](ClO_4)_2·2H_2O$: C, 42.8; H, 5.3; N, 12.8. Found: C, 43.0; H, 5.4; N, 12.8. Electron microprobe: Cl:Mn ratio 2:1. ESI mass spectrum (CH_3CN), *m/z* 958.9, $\{[Mn_2LCl_2]ClO_4\}^+$; 411.2, $\{Mn_2LCl_2\}^{2+}$; and 274.5, $\{Mn_2LCl\}^{3+}$. Selected IR bands (KBr, cm^{-1}): 3384s, 2919w, 2855w, 1608s, 1494m, 1440s, 1296m, 1149s, 1097vs, 1017s, 776m, 626m. Magnetic moment: μ_{eff}(296 K) = 5.80 μ_B per Mn(II).

Crystallography. Intensity data for colorless crystals of **1**−**3** and **4′** were measured on Siemens/Nicolet *R*3*m* and Rigaku AFC6R diffractometers, respectively. Graphite-monochromatized Mo Kα radiation, $\lambda = 0.7107$ Å, was used for **1**, **2**, and **4′**, and Cu Kα radiation, $\lambda = 1.542$ Å, for **3**. The $\omega-2\theta$ (ω for **1**) scan technique was employed such that θ_{max} was 22.5° for **1**, 27.5° for **2** and **4′**, and 60.1° for **3**. The data sets were corrected for Lorentz and polarization effects,[33] and an empirical absorption correction was applied in each case.[34] Relevant crystal data are given in Table 1.

The structures of **2** and **4′** were solved by direct methods[35,36] while those of **1** and **3** were also solved by direct methods[37] but expanded using Fourier techniques.[38] Each was refined by a full-matrix least-squares procedure based on F [34] employing reflections that satisfied

(33) Walker, N.; Stuart, D. *Acta Crystallogr., Sect. A* **1983**, *39*, 158. *XDISK: Diffractometer Data Reduction*, Version 4.20PC; Siemens Analytical X-ray Instruments Inc.: Madison, WI, 1991.
(34) *teXsan: Structure Analysis Software*; Molecular Structure Corporation, the Woodlands, TX, 1985 and 1992.
(35) Sheldrick, G. M. *SHELXS86: Program for the automatic solution of crystal structure*; University of Göttingen: Göttingen, Germany, 1986.
(36) Burla, M. C.; Camalli, M.; Cascarano, G.; Giacovazzo, C.; Polidori, G.; Spagna, R.; Viterbo, D. *J. Appl. Crystallogr.* **1989**, *22*, 389.
(37) Altomare, A.; Cascarano, M.; Giacovazzo, G.; Guagiardi, A. SIR92. *J. Appl. Crystallogr.* **1993**, *26*, 343.
(38) Beurskens, P. T.; Admiraal, G.; Beurskens, G.; Bosman, W. P.; de Gelder, R.; Israel, R.; R. O.; Smits, J. M. M. *The DIRDIF-94 Program System*; Technical Report; Crystallography Laboratory, University of Nijmegen: The Netherlands, 1994.

Table 1. Crystallographic Data for Complexes **1**−**3** and **4′**

	1	**2**	**3**	**4′**
formula	$C_{18}H_{25}Cl_2MnN_5O_4$	$C_{44}H_{66}Cl_4Mn_2N_{12}O_{10}$	$C_{39}H_{60}Cl_4Mn_2N_{10}O_{11}$	$C_{46}H_{76}Cl_4Mn_2N_{12}O_{13}$
fw	501.3	1174.8	1096.6	1256.8
space group	$P2_12_12_1$, No. 19	$P2_1/c$, No. 14	$P2_1/c$, No. 14	$P2_1/n$, No. 14
a, Å	7.959(7)	11.455(4)	13.334(2)	13.361(3)
b, Å	12.30(1)	15.037(6)	19.926(2)	16.807(5)
c, Å	21.72(2)	15.887(4)	18.799(1)	14.339(4)
β, deg		96.48(2)	104.328(8)	111.14(2)
V, Å^3	2126(3)	2719(1)	4839.4(9)	3003(1)
Z	4	2	4	2
T, K	173	293	183	180
λ, Å	0.7107 (Mo Kα)	0.7107 (Mo Kα)	1.542 (Cu Kα)	0.7107 (Mo Kα)
μ, cm^{-1}	9.07	7.25	6.85	6.64
ρ, g cm^{-3}	1.566	1.435	1.503	1.390
$R(F)$[a]	0.035	0.092	0.053	0.072
$R_w(F)$[b]	0.030	0.108	0.060	0.070

[a] $R(F) = \Sigma||F_o| - |F_c||/\Sigma|F_o|$. [b] $R_w(F) = [\Sigma(|F_o| - |F_c|)^2/\Sigma w|F_o|^2]^{1/2}$.

Table 2. Selected Bond Distances (Å) and Angles (deg) for Complexes **1**−**3** and **4′**

	1	**2**	**3**[a]	**4′**
Mn−Cl(1)	2.427(3)	2.410(2)	2.424(3) {2.417(3)}	2.420(3)
Mn−N(1)	2.253(6)	2.381(7)	2.332(8) {2.323(8)}	2.317(9)
Mn−N(2)	2.326(5)	2.280(7)	2.295(8) {2.282(8)}	2.304(9)
Mn−N(3)	2.375(6)	2.343(6)	2.333(8) {2.342(8)}	2.330(7)
Mn−N(4)	2.214(5)	2.228(6)	2.222(8) {2.194(8)}	2.23(1)
Mn−N(5)	2.261(5)	2.255(7)	2.275(8) {2.289(8)}	2.259(8)
Cl(1)−Mn−N(1)	90.1(2)	90.9(2)	93.5(2) {93.5(2)}	93.0(2)
Cl(1)−Mn−N(2)	116.6(2)	115.8(2)	119.4(2) {115.3(2)}	118.6(2)
Cl(1)−Mn−N(3)	158.4(1)	161.0(2)	160.9(2) {164.7(2)}	160.4(2)
Cl(1)−Mn−N(4)	99.8(2)	99.9(2)	95.8(2) {99.8(2)}	97.7(2)
Cl(1)−Mn−N(5)	88.6(1)	90.3(2)	90.9(2) {91.2(2)}	89.5(2)
N(1)−Mn−N(2)	76.6(2)	78.7(2)	78.5(3) {78.7(3)}	77.6(3)
N(1)−Mn−N(3)	75.4(2)	75.6(2)	76.8(3) {77.2(3)}	76.1(3)
N(1)−Mn−N(4)	117.6(2)	114.0(2)	114.4(3) {116.6(3)}	117.6(3)
N(1)−Mn−N(5)	145.4(2)	149.9(2)	148.6(3) {150.4(3)}	147.7(3)
N(2)−Mn−N(3)	76.0(2)	75.3(2)	75.3(3) {75.2(3)}	75.5(3)
N(2)−Mn−N(4)	141.4(2)	142.3(3)	142.5(3) {141.2(3)}	140.5(3)
N(2)−Mn−N(5)	73.2(2)	73.8(2)	72.4(3) {72.8(3)}	73.0(3)
N(3)−Mn−N(4)	73.9(2)	74.2(2)	74.0(3) {74.3(3)}	73.9(3)
N(3)−Mn−N(5)	112.5(2)	108.2(3)	106.1(3) {102.9(3)}	108.4(3)
N(4)−Mn−N(5)	96.7(2)	95.3(3)	96.0(3) {91.3(3)}	93.8(3)
Mn−N(1)−C(1)	103.7(4)	97.6(5)	98.5(6) {99.3(6)}	107.1(8)
Mn−N(1)−C(6)	113.9(5)	110.5(5)	110.2(6) {109.8(6}	111.2(7)
Mn−N(1)−C(19)		116.7(5)	118.1(6) {115.7(6)}	113.7(7)
Mn−N(2)−C(2)	110.5(4)	110.2(5)	109.6(6) {110.0(6)}	110.3(6)
Mn−N(2)−C(3)	104.2(4)	106.4(4)	106.8(6) {107.2(6)}	105.7(7)
Mn−N(2)−C(13)	108.4(4)	106.4(4)	106.2(6) {104.5(6)}	105.7(6)
Mn−N(3)−C(4)	111.3(4)	112.4(4)	113.0(6) {112.4(6)}	111.9(5)
Mn−N(3)−C(5)	103.4(4)	105.2(5)	102.8(6) {102.3(6)}	104.0(5)
Mn−N(3)−C(7)	106.4(4)	107.2(4)	107.5(6) {107.0(6)}	107.8(6)
Mn−N(4)−C(8)	118.9(5)	116.3(5)	116.4(7) {117.6(7)}	118.3(8)
Mn−N(4)−C(12)	121.1(4)	123.4(6)	123.8(7) {124.2(7)}	123.5(8)
Mn−N(5)−C(14)	115.8(5)	116.0(6)	116.0(7) {113.6(7)}	116.5(8)
Mn−N(5)−C(18)	124.7(5)	127.9(6)	126.4(7) {128.5(7)}	126.4(7)

[a] The halves of the binuclear cation are not identical, as is the case for **2** and **4′**, and exhibit different bond distances and angles. The values that correspond to the labeling scheme for **1**, **2**, and **4′** are listed first followed by those for the other half of the cation in brackets.

the $I \geq 3.0\sigma(I)$ criterion. Non-H atoms were generally refined with anisotropic displacement parameters, and H atoms were included in the models at their calculated positions. For **2**, the perchlorate anion was disordered and the constituent O atoms were refined isotropically. The Cl-bound O(1), O(2), and O(4) atoms were each disordered over two sites and were refined with 50% site occupancy factors. For **4′**, the two water O atoms were refined isotropically and the O(7) atom was disordered over two symmetry-related positions. The refinements were continued until convergence in each case after the inclusion of a weighting scheme of the form $1/\sigma^2(F)$. For **2** and **4′**, neither of the structure determinations is optimal owing to the quality of the crystals available for analysis. Numerous attempts to grow better crystals of these complexes proved unsuccessful. Considerable difficulties were also encountered in modeling the perchlorate anions and solvent molecules. Nevertheless, the molecular structures of the dications have been determined unambiguously. The lattice of **2** comprises dimeric dications, perchlorate anions, and DMF solvates in the ratio 1:2:2. The closest non-H contact in the lattice of 3.28(1) Å occurs between the O(5) and C(7)^i atoms, i.e., between the solvent molecule and the cation (symmetry operation i: x, $0.5 - y$, $0.5 + z$). For **4′**, the optimal refinement corresponded to a unit cell comprising dinuclear cations, perchlorate anions, DMF solvates, and water solvates in the ratio 1:2:2:1.5. The closest non-H contact in the lattice of 2.84(4) Å occurs between the water molecules and is indicative of H-bonding.

Final refinement details are collected in Table 1, selected bond lengths and angles are given in Table 2, and the atom-numbering

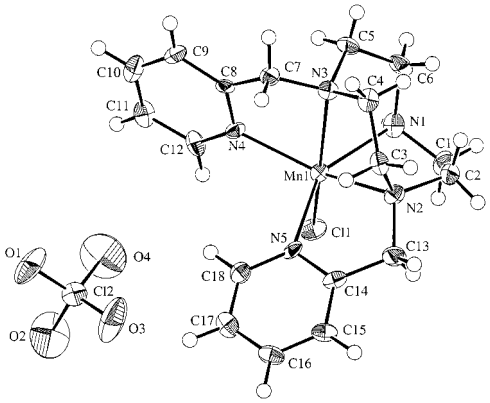

Figure 1. Molecular structure of the mononuclear cation in [Mn(dmptacn)Cl]ClO_4 (**1**) (50% probability ellipsoids) and atom-labeling scheme.

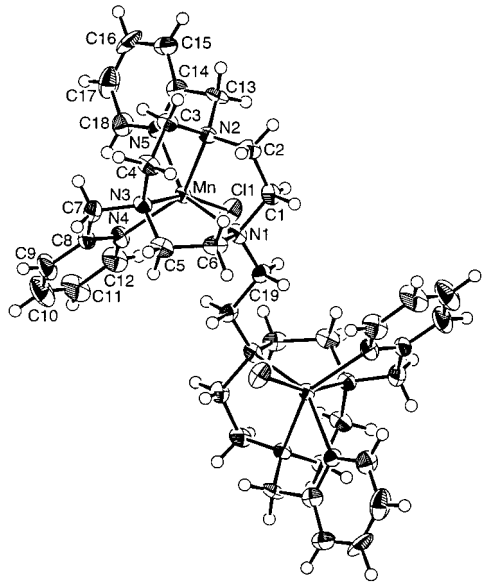

Figure 2. Molecular structure of the dinuclear cation in [Mn_2(tmpdtne)Cl_2]$(ClO_4)_2$·2DMF (**2**) (50% probability ellipsoids) and atom labeling scheme.

schemes are shown in Figures 1−4, which were drawn with ORTEP.[39] The teXsan[34] package was employed for all calculations.

Results and Discussion

Synthesis and Characterization. The mononuclear Mn(II) complex of dmptacn (**1**) and the binuclear Mn(II) complexes of tmpdtne (**2**), tmpdtnp (**3**), tmpdtnb (**4**), tmpdtn-*m*-X (**5**), and tmpdtnp-OH (**6**) were all formed by reacting the respective ligands with an excess of $MnCl_2$·$4H_2O$ in MeOH. The products were precipitated by adding $NaClO_4$ to the brown solutions and recrystallized from either DMF/H_2O or CH_3CN/H_2O mixtures to give the products as colorless crystals in 38−50% yields.

The presence of DMF in complexes **2** and **4** can be seen in the corresponding infrared spectra, which show a strong band at 1670 cm^{-1} due to the C═O group in the solvent. All complexes show bands at 1090 and 625 cm^{-1} due to the perchlorate counterions and bands in the 1400−1620 cm^{-1} region which pertain to the C═C and C═N stretching frequencies of the pyridine rings. A characteristic OH stretch at 3384 cm^{-1} is evident for **6** when the infrared spectrum is recorded in Nujol. The mononuclear complex, **1**, could be distinguished from the binuclear complexes, **2**−**6**, as it exhibited a band at 3336 cm^{-1} due to the NH stretch of the secondary amine. This is a feature of all compounds of this ligand.

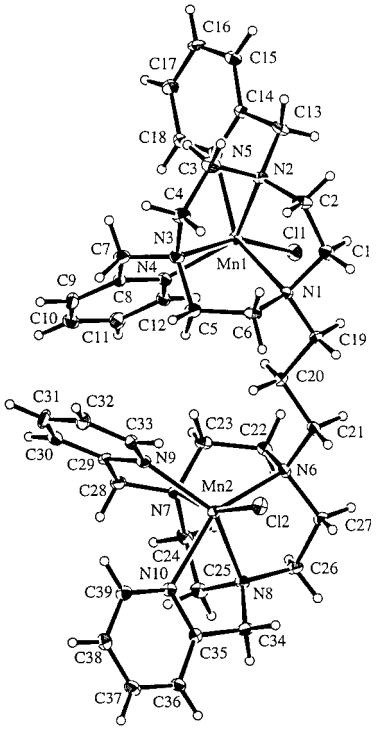

Figure 3. Molecular structure of the dinuclear cation in [Mn_2(tmpdtnp)Cl_2]$(ClO_4)_2$·$3H_2O$ (**3**) (30% probability ellipsoids) and atom-labeling scheme.

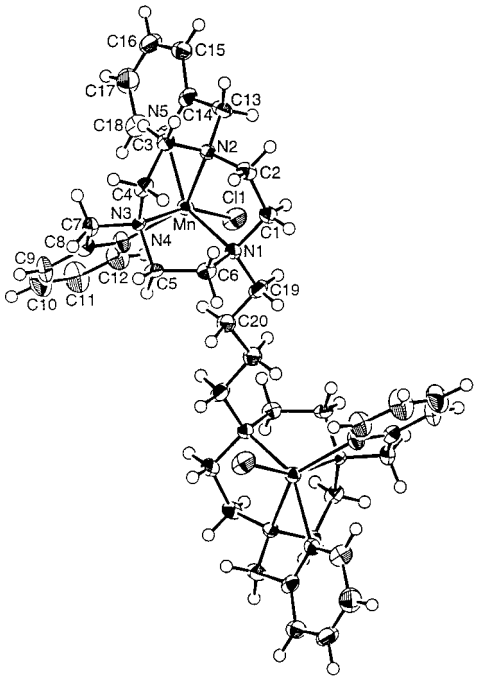

Figure 4. Molecular structure of the dinuclear cation in [Mn_2(tmpdtnb)Cl_2]$(ClO_4)_2$.4DMF·$3H_2O$ (**4′**) (50% probability ellipsoids) and atom-labeling scheme.

Crystals of **1**−**3** and **4′** grown from DMF/H_2O solutions were used to determine the molecular structure of these complexes discussed below. Although crystals of **5** and **6** were not suitable for X-ray crystallography, elemental analyses and ESI MS data indicated that these complexes were similar in composition to

(39) Johnson, C. K. *ORTEP* Report ORNL-5138; Oak Ridge National Laboratory: Oak Ridge, TN, 1976.

the others in the series. The ESI-mass spectrum of **5**, $[Mn_2(tmpdtn\text{-}m\text{-}X)Cl_2](ClO_4)_2$, showed signals at *m*/*z* 1005.2, $\{[Mn_2LCl_2]ClO_4\}^+$, and 452.2 $\{Mn_2LCl_2\}^{2+}$, while that of **6**, $[Mn_2(tmpdtnp\text{-}OH)Cl_2](ClO_4)_2$, exhibited signals at *m*/*z* 958.9, $\{[Mn_2LCl_2]ClO_4\}^+$, 411.2, $\{Mn_2LCl_2\}^{2+}$, and 274.5, $\{Mn_2LCl\}^{3+}$. These assignments were supported by the agreement between observed and simulated isotopic splitting patterns for each signal. The presence of signals attributable to $\{Mn_2LCl_2\}^{2+}$ supports the view that chloro ligands occupy the sixth Mn coordination site in **5** and **6**, as is the case for **2**−**4**.

Description of the Crystal Structures of 1−4. The molecular structure of the cation in **1**, shown in Figure 1, confirms that five coordination sites are occupied by the N donors of dmptacn while a chloride ligand completes the significantly distorted Mn(II) coordination sphere, whose geometry is intermediate between octahedral and trigonal prismatic. Although the Mn(II) center in **1** is not strictly octahedral, two possible isomers can be envisaged for the cation; viz., one isomer has the chloride ion coordinating trans to the secondary amine, whereas the other has the chloride ion coordinating cis to the secondary amine. The view of **1** shown in Figure 1 confirms that the chloride is indeed cis to the secondary amine, as does a Cl(2)−Mn(1)−N(1) angle of 90.2(2)°. The two 2-pyridylmethyl pendant arms adopt a Δ configuration, and, in contrast to those of the Cu(II) analogue, they are perpendicular rather than parallel to one another.[31] The two five-membered chelate rings formed by coordination of the 2-pyridylmethyl pendant arms to Mn(II) are puckered, as seen in the Mn(1)−N(2)−C(6)−C(5) and Mn(1)−N(4)−C(13)−C(14) torsion angles of 38.9 and 38.4°, respectively.

Several features highlight the substantial distortion in the coordination geometry of the Mn(II) center in **1**. The Mn−N bond lengths in **1** vary significantly from 2.214(5) to 2.375(6) Å and give rise to an average Mn−N bond distance (2.29 Å) that is 0.04 Å longer than that for $[Mn(tmptacn)](ClO_4)_2$, in which the Mn center adopts a pseudo-trigonal-prismatic geometry.[17] The angles subtended by the tacn nitrogens (average 76.0°) are much smaller than those subtended by the tacn ligand in the binuclear Ni(II) complex of tmpdtnb (average 84.6°), which has a more regular octahedral geometry.[40] Significantly, the tacn bite angles in **1** compare favorably with those found in $[Mn_2(Me_3tacn)_2(\mu\text{-}O_2CMe)_3]^+$ (average 76.5°)[19] and $[Mn(tmptacn)](ClO_4)_2$ (average 77.2°).[17] The distortion from a regular octahedral geometry in **1** can also be seen in the angles subtended by the five-membered chelate rings involving the tertiary amines and the pyridyl nitrogens (average 73.6°), which are also similar to those observed for $[Mn(tmptacn)](ClO_4)_2$ (average 75.4°),[17] and in the nonlinearity of the Cl(2)−Mn(1)−N(3) angle (158.4°). This degree of distortion from octahedral geometry can be quantified by the trigonal twist angle (ϑ), which is a measure of the rotation of the two N donors on the pyridyl arms and the chloro ligand relative to the tacn nitrogen donor atoms (Figure 5). For a trigonal-prismatic geometry, ϑ is 0°, while for an octahedral arrangement, ϑ is 60°. The observed value of ϑ for **1** (23.4°) confirms a geometry that it is intermediate between trigonal prismatic and octahedral but which is slightly closer to the former, as was found for $[Mn(tmptacn)](ClO_4)_2$ ($\vartheta = 19.6°$).[17] The pseudo-trigonal-prismatic geometry of the Mn(II) center in complexes of tacn-based ligands, exhibited by **1** and the related binuclear complexes **2**, **3**, and **4′** (see below), arises principally from the fact that the large Mn(II) center (0.97 Å) finds it difficult to accommodate the small tacn macrocycle on the face of an octahedron.[41] This is better achieved by metal centers with smaller ionic radii, e.g., Ni(II) and Cr(III).[41]

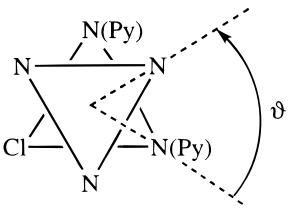

Figure 5. Definition of the trigonal twist angle (ϑ).

The binuclear cations in **2**, **3**, and **4′**, illustrated in Figures 2−4, show that ethane, propane, and butane bridges, respectively, link the two pentadentate compartments of the ligands through N(1). As was the case for **1**, the coordination sphere of each Mn(II) center is occupied by five N donors from each ligand compartment and a chloride ligand which is located cis to the bridgehead nitrogen and the Mn(II) centers adopt a pseudo-trigonal-prismatic stereochemistry (viz., ϑ is 27.3° for **2**, 26.8° for **3**, and 26.0° for **4′** and "transoid" donor angles are in the 140−160° range). In addition, the small bite angles subtended by the N donor atoms of the tacn (ca. 76°) and by the chelate rings incorporating the pyridyls (ca. 74°) match those in **1**.

Complexes **2** and **4′** adopt a true anti conformation with the two chloro ligands pointing away from each other. For these centrosymmetric complexes, the "trans" orientation of the chlorides causes the torsion angles defined by each Mn(II) center, the bridgehead nitrogen, and the two adjacent carbons in the bridge to be equal in magnitude but opposite in sign. For **2**, the torsion angles defined by Mn(1)−N(1)−C(19)−C(20) and Mn(1′)−N(1′)−C(19′)−C(20) are +62.8(8) and −62.7(8)°, respectively, while the corresponding values for **4′** are +59.6(8) and −59.5(8)°. The long Mn···Mn′ distances (6.815(3) Å for **2** and 8.279(3) Å for **4′**) are a consequence of these anti conformations. Notably, these M···M distances are respectively 0.67 and 0.40 Å shorter than those in the corresponding square-pyramidal (SP) Cu(II) complexes.[32] This reduction in M···M distance probably reflects a decrease in electrostatic repulsion attributable to the lower charge on the Mn(II) complexes (1+/Mn), when compared with the Cu(II) complexes (2+/Cu). Supporting this view is the considerably longer Ni···Ni′ distance of 9.563(4) Å found in $[Ni_2(tmpdtnb)(OH_2)_2]^{4+}$, a complex analogous to **4′** but with a higher charge per metal (2+/Ni).[40] The longer M···M separation in this Ni(II) complex (cf. **4′**), can be traced to differences in the torsion angles involving the metal, the bridgehead nitrogen and butane linker, viz., −10.9(8) and 169.1(8)°, (cf. 59.6(8) and −59.5(8)° in **4′**).

Conversion of N(1) into a tertiary nitrogen has resulted in considerable lengthening of the Mn−N(1) bond, from 2.253(6) Å in **1** to 2.381(7) Å in **2**, 2.33(1) Å (average) in **3**, and 2.317(9) Å in **4′**. The two five-membered chelate rings incorporating the 2-pyridylmethyl pendant arms in **2**, **3**, and **4′** are puckered with torsion angles that correspond to those in **1**.

The view of **3**, displayed in Figure 3, suggests that the complex adopts a syn configuration, like that observed for the Cu(II) analogue, in which the halves of the ligand are oriented toward one another. Although the "zigzag" nature of the propane bridge linking the two pentadentate compartments is maintained

(40) Brudenell, S. J.; Spiccia, L.; Bond, A. M.; Mahon, P. C.; Hockless, D. C. R. *J. Chem. Soc., Dalton Trans.* **1998**, 3919.

(41) Cotton, F. A.; Wilkinson, G. *Advanced Inorganic Chemistry*, 5th ed.; John Wiley & Sons: New York, 1988; p 745.

Table 3. Cyclic, Square-Wave, and Steady-State Voltammetric Data for Oxidation of Mn(II) Complexes in Acetonitrile (0.1 M Bu_4NClO_4) [a]

	cyclic [b]							square-wave [c]				steady-state [d]		
	$E_{1/2}$, V	ΔE_p, mV	E_p^{ox}, V	E_p^{red}, V	I_p^{ox}, μA	I_p^{red}, μA	I_p^{ox}/I_p^{red}	E_p V	$W_{1/2}$ V	I_p μA	$E_{1/2}$ V	$E_{1/4}-E_{3/4}$ mV	I_L nA	$10^{-6}D$ cm^2 s^{-1}
1	0.41	66	0.45	0.38	3.3	3.2	0.97	0.41	0.10	6.1	0.41	59	5.7	12.3
								1.03	0.18	3.4				
2	0.54	128	0.61	0.48	5.0	4.9	0.98	0.54	0.16	17.9	0.54	89	8.6	9.5
								1.30	0.17	11.4				
								1.38 sh		5.2				
3	0.51	72	0.55	0.48	5.9	5.9	1.00	0.51	0.10	17.2	0.51	50	8.1	8.7
								1.26	0.14	13.0				
4	0.49	78	0.53	0.46	5.4	5.2	0.96	0.49	0.10	21.9	0.49	58	8.1	8.8
								1.24	0.12	20.0				
5	0.51	110	0.53	0.42	5.0	4.9	0.98	0.51	0.12	18.0	0.51	70	8.0	8.5
								1.28	0.11	16.5				
6	0.52	78	0.56	0.48	5.3	5.5	1.04	0.52	0.09	12.8	0.52	63	7.3	7.8
	0.88	64	0.92	0.85	3.8	3.8	1.00	0.89	0.10	7.2	0.89	59	3.8	
								1.33	0.10	7.2				

[a] Potentials are quoted with respect to the Fc/Fc^+ couple. The concentrations of the complexes used were in the range 0.5−0.55 mM, but the current data in the table are normalized to 0.5 mM to facilitate comparison of values. [b] Cyclic voltammetric data were measured at a scan rate of 100 mV s^{-1}. [c] Square-wave voltammetric data were measured with a period of 30 ms. [d] Steady-state voltammetric data were measured on a 25 μm radius Pt microdisk electrode.

in both complexes, as this is sterically preferred for this ligand, it is electrostatically unfavorable for the chlorides to be situated near each other. Consequently, **3** adopts an anti configuration, which minimizes Cl···Cl repulsion.

The N(1)−C(19)−C(20)−C(21) and N(6)−C(21)−C(20)−C(19) torsion angles of −8.7(8) and −3.5(8)°, respectively, show an approximately all-gauche arrangement for the atoms of the bridge in **3**. Thus, the orientation of **3** (Figure 4) is a result of each pentadentate compartment twisting around the bridgehead nitrogens, N(1) and N(6), without torsional distortion of the bridge itself. The degree of this twisting is reflected in the Mn(1)−N(1)−C(19)−C(20) and Mn(2)−N(6)−C(21)−C(20) torsion angles of −62.8(8) and −61.6(8)°, respectively, which confirm that even though the chlorides in **3** are directed away from one another, the metals are on the same side of the ligand. In contrast, the corresponding torsion angles of +62.7(8) and −62.7(8)° for **2** highlight the true anti orientation of this complex. The "closed" arrangement of **3** leads to an Mn···Mn′ separation of 6.797(2) Å, which is similar to that in **2** (6.815(3) Å).

Magnetic Properties and ESR Spectra. The room-temperature magnetic moments, μ_{eff} (per Mn^{II}), of **1**−**6** ($5.80 \le \mu_{eff} \le 5.94\ \mu_B$) are typical of high-spin Mn(II) complexes.[15,17,42] Variable-temperature magnetic susceptibility measurements (4.5−296 K) of **2**−**6** showed no evidence of coupling between the two Mn(II) centers. This reflects the quite large Mn···Mn separations (≥6.8 Å) and absence of bridging units capable of mediating such interactions.

The ESR spectra of **1**−**6**, recorded as frozen DMF solutions at 99 K, are typical of uncoupled or very weakly coupled Mn(II) complexes[43,44] with a zero-field interaction of $D \approx 0.09$ cm^{-1}. Apart from a minor, sharp 6-line signal centered at $g = 2.00$ (peak separation ∼ 90 G) due to small amounts of Mn^{2+} impurity, the complexes display very broad resonances, which are typical of low-symmetry Mn(II) complexes, as was found for $[Mn([9]aneN_2S)_2](ClO_4)_2$ ([9]aneN$_2$S = 1-thia-4,7-diazacyclononane) and $[Mn(tacn)_2](ClO_4)_2$.[42] The large spectral line widths are a consequence of the distorted Mn(II) geometries, which for complexes **1**−**4** are intermediate between trigonal prismatic and octahedral in the solid state.

Electrochemistry. The redox behavior of **1**−**6** has been studied by cyclic (CV), square-wave (SWV), and steady-state voltammetry (SSV). The CV trace of the mononuclear complex, $[Mn(dmptacn)Cl]^+$, **1**, displays a chemically reversible wave at a scan rate of 100 mV s^{-1} ($I_p^{ox}/I_p^{red} = 0.97$) for which $E_{1/2} = +0.41$ V (vs Fc/Fc^+). This $E_{1/2}$ value is assumed to be the reversible potential because it is in agreement with the E_p and $E_{1/2}$ values obtained from SWV and SSV, respectively (Table 3). This initial oxidation reaction corresponds to the 1e$^-$ oxidation of Mn(II) to Mn(III) shown in eq 1, with SSV data giving a diffusion coefficient of 12.3×10^{-6} cm^2 s^{-1}.

$$Mn^{II} \rightleftharpoons Mn^{III} + e^- \qquad (1)$$

At much more positive potentials, another redox process is just visible in the CV trace of **1** but is masked by additional ill-defined (possibly ligand-based) oxidative processes that become apparent above +1.0 V. However, this process is clearly identifiable in the SWV trace from which an E_p value of +1.03 V could be determined. The $W_{1/2}$ value is broader than the initial process and the peak height is smaller indicating irreversibility is present. The SWV data signifies a further 1e$^-$ oxidation of the Mn(III) center to Mn(IV) followed by a fast decomposition reaction, as shown in eq 2.

$$Mn^{III} \rightleftharpoons Mn^{IV} + e^- \xrightarrow{\text{very fast}} \text{products} \qquad (2)$$

Typical responses for complexes **2**, **3**, and **6** are displayed in Figures 6−8. As for the mononuclear complex, two oxidation waves also are observed in the CV and SWV of the binuclear complex $[Mn_2(tmpdtne)Cl_2]^{2+}$, **2** (Figure 6). The CV responses show that the first process is chemically reversible. However, the shape of this wave and the current magnitudes under CV, SWV, and SSV conditions indicate that the two Mn(II) centers are each oxidized in a reversible one-electron process at slightly different potentials, as was found for the Ni(II) analogue.[40] The first overall reversible two-electron oxidation process in **2** ($I_p^{ox}/I_p^{red} = 0.98$) occurs at an average $E_{1/2}$ value of +0.54 V. The fact that this is not a simple reversible 2e$^-$ process is evidenced by the large ΔE_p (128 mV) and $W_{1/2}$ (0.16 V) values (Table 3).

(42) Gahan, L. R.; Grillo, V. A.; Hambley, T. W.; Hanson, G. R.; Hawkins, C. J.; Proudfoot, E. M.; Moubaraki, B.; Murray, K. S.; Wang, D. *Inorg. Chem.* **1996**, *35*, 1039.
(43) Mathur, P.; Crowder, M.; Dismukes, G. C. *J. Am. Chem. Soc.* **1987**, *109*, 5227.
(44) Mathur, P.; Dismukes, G. C. *J. Am. Chem. Soc.* **1983**, *105*, 7093.

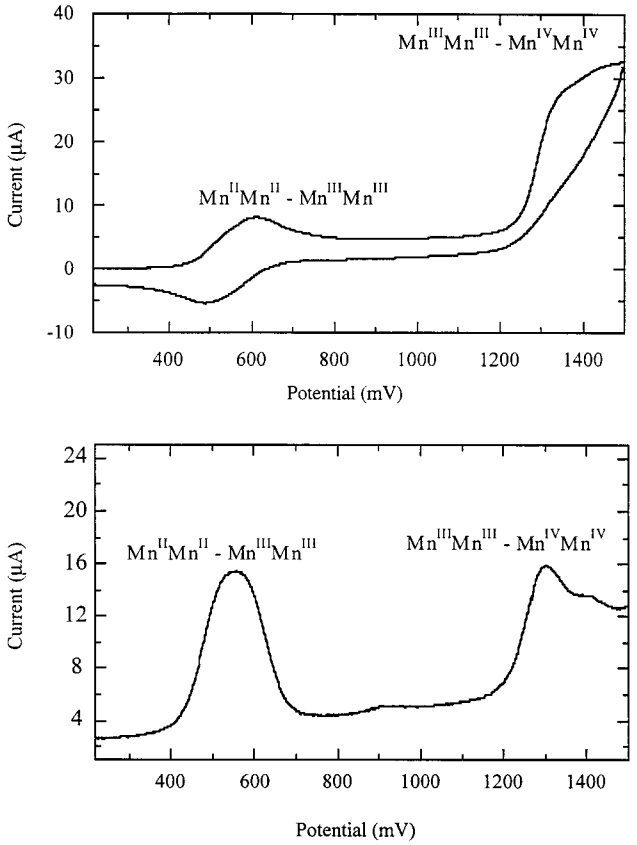

Figure 6. Cyclic (scan rate 100 mV s^{-1}) and square-wave (period 30 ms) voltammograms of **2**, measured at 20 °C in acetonitrile (0.1 M Bu_4NClO_4) using an 0.8 mm Pt macrodisk electrode. The potential axis used is relative to the Fc/Fc^+ couple.

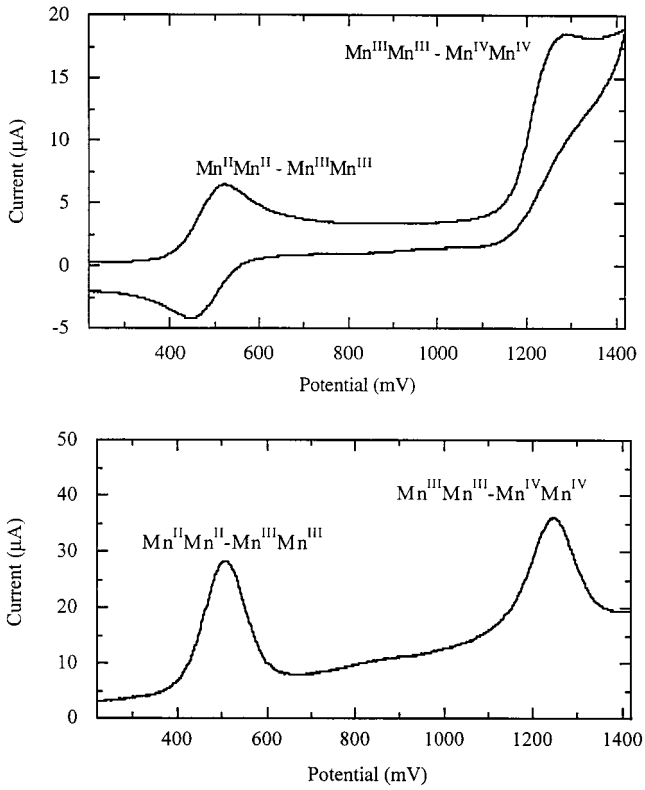

Figure 7. Cyclic (scan rate 100 mV s^{-1}) and square-wave (period 30 ms) voltammograms of **4**, measured at 20 °C in acetonitrile (0.1 M Bu_4NClO_4) using an 0.8 mm Pt macrodisk electrode. The potential axis used is relative to the Fc/Fc^+ couple.

That is, the two Mn(II) centers in **2** are close enough to electronically influence one another, so that oxidation of the first Mn(II) center renders oxidation of the second Mn(II) center more difficult. Thus, the first oxidation wave of **2** involves two closely separated $1e^-$ processes represented by eq 3 with a separation in the reversible potential of ca. 40 ± 10 mV.

$$Mn^{II}Mn^{II} \rightleftharpoons Mn^{III}Mn^{II} + e^- \rightleftharpoons Mn^{III}Mn^{III} + e^- \quad (3)$$

The combination of CV and SWV peak heights and of SSV limiting current data, displayed in Table 3, in conjunction with the calculated diffusion coefficient enables confirmation that the initial voltammetric responses for **2** and the other binuclear complexes, **3**−**6**, involve two electrons, as opposed to the one-electron process observed for **1**. That is, all data sets when used with the relevant theory give internally consistent data under this assumption. Thus, for example, the greater value of D for the mononuclear complex, **1** (12.3×10^{-6} cm^2 s^{-1}), when compared with those of the binuclear complexes (average 8.7×10^{-6} cm^2 s^{-1}) is as expected, since the larger binuclear molecules would normally diffuse to the electrode surface more slowly than **1**. In addition, since the theory for a reversible linear-sweep voltammogram[45] predicts that $I_p \propto n^{3/2}D^{1/2}$, the peak currents per unit concentration for the binuclear complexes ($n = 2$) should be greater than those for **1** ($n = 1$), as is found experimentally (Table 3).

The second oxidation wave in the cyclic voltammogram of **2** is partly masked and complex, suggesting ill-defined processes possibly involving oxidation of the ligand. These background processes were also observed in the CV trace of the free ligand tmpdtne. In the SWV trace of **2**, there is one major wave with an E_p value of +1.30 V and a minor wave at +1.38 V probably arising from a decomposition reaction associated with the generation of $Mn^{IV}Mn^{IV}$. Thus, the Mn(III) centers in **2** are oxidized via two very closely spaced $1e^-$ processes with the Mn^{IV} state being very reactive, as in the case with the monomer, as shown in eq 4. The current magnitude for the major process is consistent with this being a $2e^-$ process.

$$Mn^{III}Mn^{III} \rightleftharpoons Mn^{IV}Mn^{III} + e^- \rightleftharpoons Mn^{IV}Mn^{IV} + e^- \xrightarrow{\text{very fast}} \text{product(s)} \quad (4)$$

All three voltammetric techniques corroborate the respective $E_{1/2}$ and E_p values of +0.51 and +0.49 V recorded for the first chemically reversible oxidation responses of **3** and **4** ($I_p^{ox}/I_p^{red} = 1.0$). CV signals for **3** and **4** (Figure 7) are relatively sharp compared to those for **2**, as evidenced by the smaller ΔE_p values of 72 and 78 mV, respectively, and the sharper peaks in the SWV's. However, these ΔE_p values are still larger than expected for a simultaneous $2e^-$ process (i.e., $\Delta E_p = 57$ mV/n), indicating that oxidation of the two Mn(II) centers to Mn(III) occurs via two closely spaced $1e^-$ processes, as shown by eq 3, but with a separation of 25 ± 10 mV. These results are consistent with those obtained for the Cu(II) and Ni(II) analogues.[32,40] The diffusion currents for **3** and **4** (SSV, $I_L = 8.1$ nA, where D(av) $= 8.8 \times 10^{-6}$ cm^2 s^{-1}) are similar to that of **2** (SSV, $I_L = 8.6$ nA, where $D = 9.3 \times 10^{-6}$ cm^2 s^{-1}), for which the first oxidation process also involves two electrons. According to the SWV data, the second overall but chemically reversible oxidation processes for **3** and **4**, represented by eq 4, are observed at

(45) Bard, A. J.; Faulkner, L. R. *Electrochemical Methods*; John Wiley & Sons: New York, 1980.

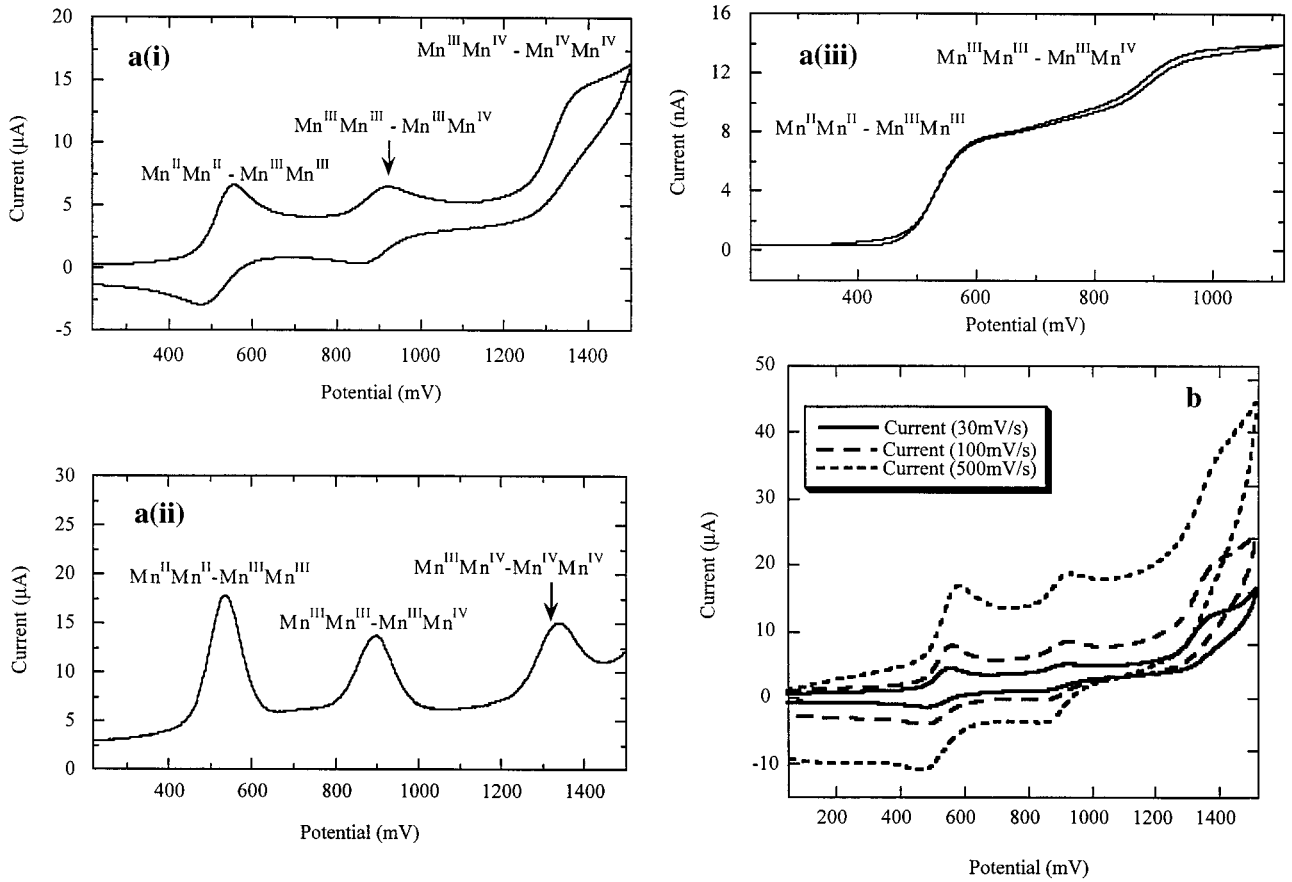

Figure 8. (a) Cyclic ((i) scan rate 100 mV s^{-1}) and square-wave ((ii) period 30 ms) voltammograms of **6**, measured using an 0.8 mm Pt macrodisk electrode, and steady-state (iii) voltammograms, measured on a 25 μm radius Pt microdisk electrode, in acetonitrile (0.1 M Bu_4NClO_4) at 20 °C. (b) Variable-scan-rate cyclic voltammograms of **6**. The potential axis used is relative to the Fc/Fc^+ couple.

less positive average $E_{1/2}$ values of 1.26 and 1.24 V, respectively, than that for **2** (1.30 V).

In the case of the tmpdtn-*m*-X complex, **5**, the three electrochemical methods have established an $E_{1/2}$ value of +0.51 V for the first unresolved $2e^-$ oxidation process, while SWV gave an $E_{1/2}$ value of +1.28 V for the second $2e^-$ oxidation. However, relative to the traces of **3** and **4**, the CV trace for **5** is significantly broadened (viz., a large ΔE_p value of 110 mV) with a small broadening of the corresponding SWV and SSV signals being observed relative to **3** and **4**. The behavior of **5** is intermediate among those of **2**, **3**, and **4** with respect to separations in potentials.

The average $E_{1/2}$ values for the first unresolved $2e^-$ oxidation responses of **2**−**4**, decrease with increasing chain length (i.e., $E_{1/2}$ = +0.54, +0.52, and +0.49 V, respectively) as do those for the second oxidation (i.e., +1.34, +1.26, and +1.24 V, respectively). These findings support the postulate that, as the alkyl chain is shortened, the metal centers exert greater electrostatic influence on one another, so that oxidation of one metal center is affected by the increased positive charge on the other. These influences diminish as the length of the bridging unit and Mn···Mn separation increase, and the complexes become easier to oxidize. The ease of oxidation of the mononuclear complex, **1** ($E_{1/2}$ values of +0.41 and +1.03 V), in part reflects the absence of electrostatic effects that would be caused by a second metal center. There are also differences in ligand field strength, since in the binuclear complexes, **2**−**6**, three tertiary tacn nitrogens coordinate to each Mn center whereas in the mononuclear complex the ligand will have a higher field strength since a secondary nitrogen replaces the bridgehead nitrogen. This results in a relative stabilization of the higher Mn oxidation states. Data for the $[Mn(dtne)]^{2+/3+}$ and $[Mn(tacn)_2]^{2+/3+}$ redox couples support this interpretation.[15] The potential for the dtne complex, incorporating two tertiary nitrogens, is +0.3 V more positive than that for the tacn complex, which contains no tertiary nitrogens.

Compound **5** does not follow the above trend, and despite having a longer carbon chain length linking the halves of the ligands leading to the expectation of a longer Mn···Mn separation, it displays an average $E_{1/2}$ value that is slightly more positive than that for **4**. The aromatic bridging unit may be reducing the binding ability of the bridgehead nitrogen and hence the overall field strength of the ligand, and this could be making oxidation more difficult. The $E_{1/2}$ values for **5** follow the trend observed for the analogous Ni(II) complex. However, any interpretation of these data must necessarily be tentative, since the process need not comprise purely EE reactions.[32, 45]

The electrochemical behavior of the binuclear complex of tmpdtnp-OH, **6**, is quite different from those of **1**−**5** in that three rather than two oxidation processes are clearly present (Figure 8). The first oxidation, observed at $E_{1/2}$ = +0.52 V according to the three voltammetric techniques (Table 3), is attributed to two unresolved $1e^-$ processes in which both Mn(II) centers are oxidized to the Mn(III) state, as seen earlier in eq 3. The second response, observed at $E_{1/2}$ = +0.89 V, is proposed to involve a $1e^-$ oxidation of the $Mn^{III}Mn^{III}$ complex to the mixed-valent $Mn^{III}Mn^{IV}$ complex. At the more positive potential of +1.33 V, there is a further $1e^-$ process corresponding to the formation of the $Mn^{IV}Mn^{IV}$ complex. Both the ΔE_p value of 78 mV and the I_p^{ox} and I_p^{red} values of 5.3 and 5.5 μA,

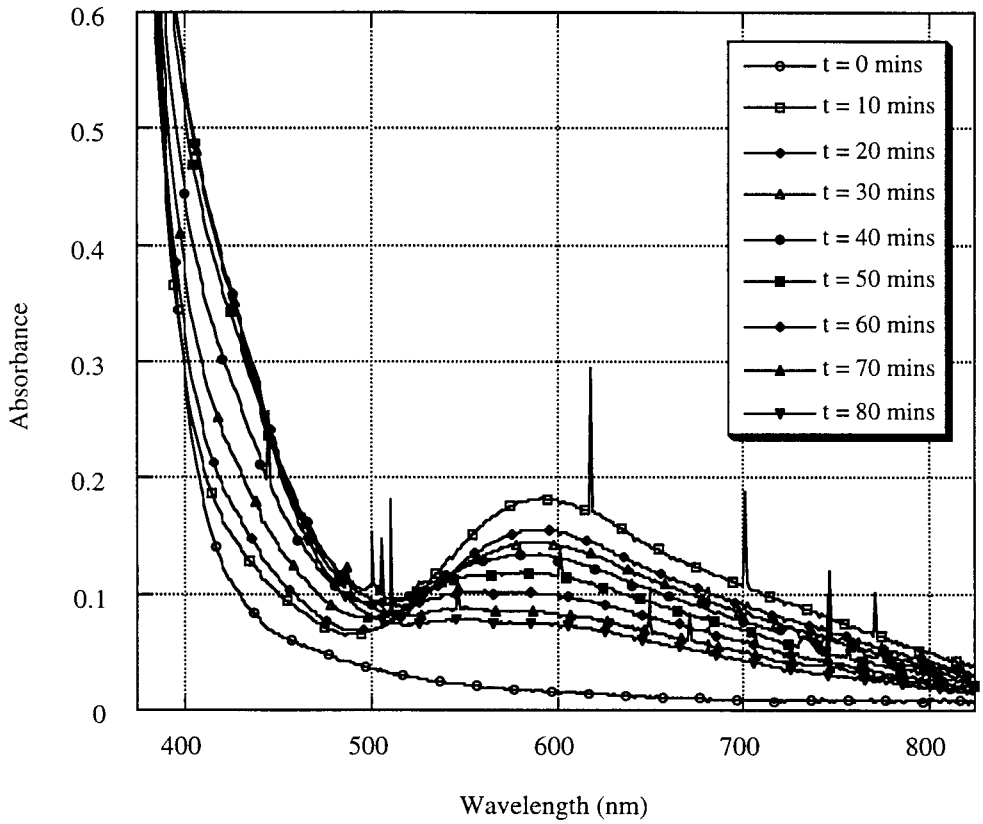

Figure 9. UV−visible spectra of a DMF solution of **4** ([complex] ~ 5 mM) measured at 10 min intervals after the addition of hydrogen peroxide ([H_2O_2] ~ 1.5 M).

respectively (Table 3), provide strong evidence that the first oxidation process of **6** involves two closely spaced 1e$^-$ steps. These values compare particularly well with those of **3** (ΔE_p = 72 mV; I_p^{ox} and I_p^{red} = 5.9 μA), which correspond to two overlapping 1e$^-$ oxidation processes. Assignment of the second process as a reversible 1e$^-$ oxidation process is based on the close match of the I_p^{ox} and I_p^{red} values (3.8 μA, Table 3) with those of **1** (I_p^{ox} and I_p^{red} = 3.3 and 3.2 μA), a compound known to undergo 1e$^-$ oxidation to Mn(III), and also on the fact that the I_p value of 7.1 μA determined for this process by SWV (see Table 3) is about half that recorded for the first 2e$^-$ oxidation (I_p = 12.5 μA). Moreover, the diffusion current determined from the SSV trace for the first process (I_L = 7.3 nA) is also about twice that for the second process (I_L = 3.8 nA). Thus, the evidence is consistent with the assignment of the first process as a two-electron oxidation and the second as a one-electron process generating a mixed-valent $Mn^{III}Mn^{IV}$ species. Since the shape and height of the third process observed in the SWV of **6** (i.e., $W_{1/2}$ = 0.10 and I_p = 7.1 μA) closely match those of the second process, it can be concluded that the third oxidation process in **6** also corresponds to a 1e$^-$ step, to give an $Mn^{IV}Mn^{IV}$ complex which then rapidly decomposes to an unknown species. The variable-scan-rate CV traces for **6** (Figure 8b) show the expected variation in peak currents with the square root of the scan rate. This would not be expected if competing kinetic processes were occurring on the electrochemical time scale, and were contributing to the electrochemical responses.

The $Mn^{III}Mn^{III} \rightarrow Mn^{III}Mn^{IV} \rightarrow Mn^{IV}Mn^{IV}$ type of redox behavior proposed for **6** has also been observed for binuclear Mn(III) complexes of the type $[Mn(III)_2L_2(\mu\text{-}OH)(\mu\text{-}CH_3CO_2)_2]^{2+}$, where L = an N-substituted tacn macrocycle.[25] The binuclear complexes exhibit two oxidation processes corresponding to the $Mn^{III}Mn^{III} \rightarrow Mn^{III}Mn^{IV}$ oxidation around +0.6 to +1.0 V and to the $Mn^{III}Mn^{IV} \rightarrow Mn^{IV}Mn^{IV}$ oxidation around +1.2 to +1.5 V, which is consistent with the interpretation of the data for the second and third processes for **6**, in which the processes at +0.89 and +1.33 V are assigned to the formation of $Mn^{III}Mn^{IV}$ and $Mn^{IV}Mn^{IV}$ species, respectively. Following oxidation of **6** to the $Mn^{III}Mn^{III}$ complex, an alkoxide bridge could link the two Mn centers through deprotonation and coordination of the central oxygen of the ligand, thus enabling formation of an alkoxo-bridged $Mn^{III}Mn^{IV}$ complex (Scheme 2). Since such a process involves substitution at Mn(III), a d^4 system that is subject to Jahn−Teller distortion, this process may be so fast that no evidence for it is found in the variable-scan-rate CV traces. The X-ray structure of the alkoxide-bridged binuclear Zn(II) complex[46] demonstrates that two metal centers can be bridged by a deprotonated tmpdtnp-OH ligand. Furthermore, Wieghardt and co-workers[29] recently reported binuclear $Mn^{II}Mn^{III}$, $Mn^{III}Mn^{III}$, and $Mn^{III}Mn^{IV}$ complexes of the related Me_4dtnp-OH ligand which included a mixed-valent complex, $[Mn^{III}Mn^{IV}(Me_4dtnp\text{-}O)(PhCO_2)(PhBO_2)]^{3+}$, in which the oxygen of the deprotonated ligand bridged the Mn centers.

Reactions with Hydrogen Peroxide. Interest in the disproportionation of hydrogen peroxide by Mn enzymes,[3,7,8] and in the ability of Mn catalysts (including complexes of tacn and its derivatives) to enhance the bleaching properties of peroxide[12a] has led us to explore the reaction of complexes **1**−**6** with excess H_2O_2 (typically >1000-fold). Our initial qualitative examination of this reaction revealed that addition of H_2O_2 to DMF solutions of **1**−**6** causes the vigorous evolution of dioxygen coupled with distinct color changes (see below). This finding was surprising

(46) Brudenell, S. J.; Spiccia, L.; Hockless, D. C. R.; Tiekink, E. R. T. *J. Chem. Soc., Dalton Trans.* in press.

Scheme 2

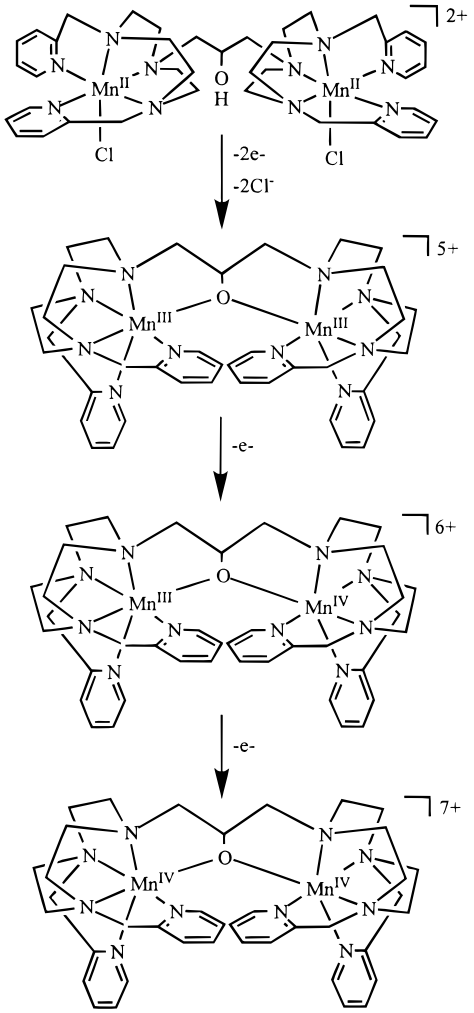

at first, since it was anticipated that these complexes may have been too coordinatively saturated to exhibit such reactivity; viz., five coordination sites are occupied by the strongly binding N_5 ligand chromophore. The behavior of complexes **1**−**6** is similar to that of bridged binuclear Mn complexes that sustain many H_2O_2 disproportionation cycles.[7,24,43,47] For many of these systems, although a substantial number of turnovers have been achieved, activity does diminish. Protonation of the ligand followed by dissociation of the complex through release of Mn^{2+} is one way by which reactivity can be reduced and ultimately lost.[7] For **1**−**6**, the growth of the $[Mn(OH_2)_6]^{2+}$ ESR signal and precipitation of MnO_2 indicate that these complexes dissociate during cycling.

For **1**, **2**, **5**, and **6**, DMF solutions of the complexes changed from colorless to brown within 5 min of the addition of H_2O_2. After 3 h, the solutions were almost colorless, the evolution of oxygen had ceased, and small amounts of MnO_2 had deposited. Further evolution of oxygen was observed on addition of more hydrogen peroxide. In contrast, addition of hydrogen peroxide to **3** and **4** resulted in a more dramatic series of color changes, viz. colorless to pale blue within minutes, to pale green after 30 min, to brown after 90 min, and back to almost colorless after 3 h. The time-dependent variation of the UV−visible spectrum of **4** is shown in Figure 9 ([complex] $\sim 5 \times 10^{-3}$ M, initial $[H_2O_2] \sim 1.5$ M). A blue solution is generated within

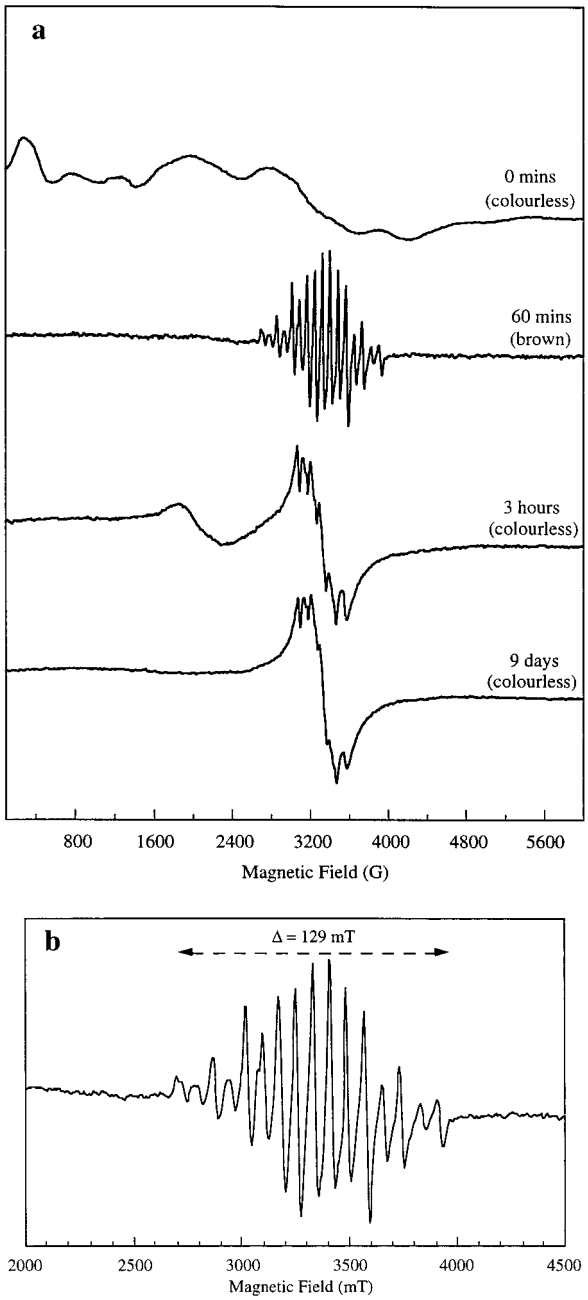

Figure 10. Frozen-solution (99 K) ESR spectra of a DMF solution of **2** ([complex] $\sim$ 1 mM) measured at various times after the addition of hydrogen peroxide ($[H_2O_2] \sim 1.5$ M) and (b) an expansion of the 16-line ESR spectrum observed after 60 min.

minutes, exhibiting an absorption maximum at 590 nm that may be due to a transition within an oxo- or peroxo-bridged Mn intermediate. As the color of the solution changes to light brown, the intensity of this band diminishes and a shoulder appears at ca. 450 nm, typical of a high-valent Mn complex and possibly oxo (or even peroxo) Mn^{IV} complexes.[1,19,25,48] ESR measurements exclude the formation of mixed-valent intermediates, either $Mn^{II}Mn^{III}$ or $Mn^{III}Mn^{IV}$ species, as these give rise to distinct, intense signals. Indeed, the ESR spectra of **1** and **3**−**6** recorded in frozen DMF at various times following the addition of peroxide showed only an enhancement of the 6-line $[Mn(OH_2)_6]^{2+}$ signal centered at 3300 G (peak separation = 90 G). Since some oxidation states of Mn are ESR inactive (e.g., the Mn(III) ion is generally ESR silent owing to rapid electron

(47) Delroisse, M.; Rabion, A.; Chardac, F.; Tetard, D.; Verlhac, J.-B.; Fraisse, L.; Seris, J.-L. *Chem. Commun.* **1995**, 949.

(48) Mandal, S. K.; Armstrong, W. H. *Inorg. Chim. Acta* **1995**, *229*, 261.

relaxation rates and large zero-field spitting[49]), the task of accurately assigning the UV−visible absorption bands to specific oxidation states is difficult.

In contrast to complexes **1** and **3**−**6**, the binuclear complex of tmpdtne, **2**, produces a very distinct 16-line ESR signal following reaction with excess H_2O_2 (Figure 10). The signal disappears after 3 h, and a signal due to $[Mn(OH_2)_6]^{2+}$ appears. The 16-line response is associated with a color change from colorless to brown and indicates the formation of a mixed-valent species. While it should be noted that $Mn^{II}Mn^{III}$ species can give rise to similar multiline ESR signals,[20,22,29,43] the signal for **2** is most likely due to an $Mn^{III}Mn^{IV}$ complex. An expanded view of the signal (Figure 10b) shows that it is centered at 3300 G ($g = 2.0$) and that it closely matches the 16-line ESR spectrum often observed for μ-oxo-bridged $Mn^{III}Mn^{IV}$ dimers.[1,12a,16,29,50−53] Such complexes are strongly antiferromagnetically coupled with an $S = {}^1/_2$ ground state. The signal width of $\Delta = 129$ mT for **2** falls within the range for $Mn^{III}Mn^{IV}$ complexes of 110−135 mT[12,29,50] and is distinguishable from those of mixed-valent Mn^{II}-Mn^{III} complexes, which are in the range of 160−180 mT.[20,22,29,43]

Since an Mn···Mn separation of 2.531 Å was observed for the bis(μ_2-oxo) μ-peroxo Mn^{IV} complex, $[(Me_3tacn)_2Mn_2(\mu_2\text{-}O)_2(\mu\text{-}O_2)]^{2+}$,[21] it may have been anticipated that, due to the large Mn···Mn separation of 6.815(3) Å observed in the solid-state structure of **2**, the formation of a similar complex would be precluded. However, the related bis(tridentate) ligand Me_4-dtne (1,2-bis(4,7-dimethyl-1,4,7-triazacyclonon-1-yl)ethane), in which the two macrocycles are linked by an ethane bridge identical to that in tmpdtne, forms a mixed-valent complex, $[Mn^{III}Mn^{IV}(\mu\text{-}O)_2(\mu\text{-}CH_3COO)Me_4dtne]^{2+}$, and produces a 16-line ESR spectrum like that of **2**,[12a] as does the $[Mn^{III}Mn^{IV}(\mu\text{-}O)(\mu\text{-}O_2CPh)(\mu\text{-}O_2BPh)]^{n+}$ complex of Me_4dtnp-OH.[29] This not only supports the assignment of the $Mn^{III}Mn^{IV}$ state for the 16-line signal of **2** but also demonstrates that oxo-bridged complexes can be supported by ethane-linked bis(1,4,7-triazacyclononane) ligands. Notably, Tolman and co-workers[54] have very successfully used alkyl- and xylyl-linked bis(1,4,7-triazacyclononane) ligands to support the high-valent $[Cu^{III}_2O_2]^{2+}$ cores with quite short Cu···Cu distances. In the present system, oxidation of the $Mn^{II}Mn^{II}$ complex to the $Mn^{III}Mn^{III}$ state is electrochemically facile. Since Mn^{III} is expected to be labile, rapid replacement of some N donors with harder O donors (e.g., from H_2O) would introduce groups capable of bridging the Mn centers.

Conclusion

The series of binuclear Mn(II) complexes, **2**−**6**, reported here represent an important addition to the rapidly expanding catalog of manganese complexes. The molecular structures of four of the complexes confirmed that the geometries about each metal center were intermediate between trigonal prismatic and octahedral. Electrochemical measurements indicated that as the metal−metal separation increased, electrostatic repulsions were reduced and oxidation of the complexes occurred at lower potentials. Two $2e^-$ oxidation processes, corresponding to Mn^{II}-$Mn^{II} \rightarrow Mn^{III}Mn^{III}$ and $Mn^{III}Mn^{III} \rightarrow Mn^{IV}Mn^{IV}$, were observed for complexes **2**−**5** and on closer examination were found to consist of two overlapping $1e^-$ processes, such that the Mn^{II}-Mn^{III} and $Mn^{III}Mn^{IV}$ species were generated before being oxidized further to the $Mn^{III}Mn^{III}$ and $Mn^{IV}Mn^{IV}$ forms, respectively. Complex **6** forms a mixed-valent $Mn^{III}Mn^{IV}$ intermediate at a much lower potential than **2**−**5**. Bridging of the two Mn centers through an endogenous propoxide bridge could be responsible for this behavior. Preliminary results indicate that complexes **1**−**6** catalyze the disproportionation of H_2O_2 and that an oxo-bridged mixed-valent Mn intermediate is formed in the case of **2**.

Acknowledgment. This work was supported by the Australian Research Council (L.S., A.M.B., E.R.T.T.). S.J.B. was the recipient of a Monash Graduate Scholarship. We thank Professor K. S. Murray and Dr. B. Moubaraki for carrying out the low-temperature magnetic susceptibility measurements and Professor J. Pilbrow for access to ESR facilities.

Supporting Information Available: X-ray crystallographic files in CIF format, for **1**−**3** and **4′**. This material is available free of charge via the Internet at http://pubs.acs.org.

IC9814470

(49) Drago, R. S. *Physical Methods in Chemistry*; Saunders: Philadelphia, PA, 1977.
(50) Hagen, K. S.; Armstrong, W. H.; Hope, H. *Inorg. Chem.* **1988**, *27*, 969.
(51) Tan, X.-L.; Gultneh, Y.; Sarneski, J. E.; Scholes, C. P. *J. Am. Chem. Soc.* **1991**, *113*, 7853.
(52) Frapart, Y.-M.; Boussac, A.; Albach, R.; Anxolabehere-Mallart, E.; Delroisse, M.; Verlhac, J.-B.; Blondin, G.; Girerd, J.-J.; Guilhem, J.; Cesario, M.; Rutheford, A. W.; Lexa, D. *J. Am. Chem. Soc*. **1996**, *118*, 2669.
(53) Lal, T. K.; Mukeherjee, R. *Inorg. Chem.* **1998**, *37*, 2373.
(54) Tolman, W. B. *Acc. Chem. Res*. **1997**, *30*, 227 and references therein.